NANOPARTICLES

Unraveling structures of protection ligands on gold nanoparticle $Au_{68}(SH)_{32}$

Wen Wu Xu,[1] Yi Gao,[1,2]* Xiao Cheng Zeng[2]*

New low-energy atomic structures of the thiolate-protected gold nanoparticle $Au_{68}(SH)_{32}$ are uncovered, where the atomic positions of the Au atoms are taken from the recent single-particle transmission electron microscopy measurement by Kornberg and co-workers, whereas the pattern of thiolate ligands on the gold core is attained on the basis of the generic formulation (or rule) of the "divide and protect" concept. Four distinct low-energy isomers, Iso1 to Iso4, whose structures all satisfy the generic formulation, are predicted. Density-functional theory optimization indicates that the four isomers are all lower in energy by 3 to 4 eV than the state-of-the-art low-energy isomer reported. Further analysis of the optimized structures of $Au_{68}(SH)_{32}$ shows that the structure of gold core in Iso1 to Iso4 is consistent with the experiment, whereas the positions of a few Au atoms at the surface of gold core are different. The computed optical absorption spectra of the four isomers are consistent with the measured spectrum. Computation of catalytic properties of $Au_{68}(SH)_{32}$ toward CO oxidation suggests that the magic number cluster can be a stand-alone nanoscale catalyst for future catalytic applications.

INTRODUCTION

Highly stable thiolate-protected gold nanoparticles (RS-AuNPs) can be viewed as "super atoms" for making cluster-assembled materials whose novel properties may be exploited for applications in catalysis, nanotechnology, or chemical biology. Determination of the structures of RS-AuNPs in the range of 1 to 2 nm has attracted considerable research interests over the past two decades (1–9). In the laboratory, the most common approach to determine the structures of the RS-AuNPs is x-ray crystallography. However, a critical prerequisite for using the x-ray crystallography technology is to achieve a sizable single crystal of the RS-AuNPs, which generally is a very challenging task. To date, only the structures of the following RS-AuNPs have been fully resolved by x-ray crystallography: $Au_{102}(p\text{-MBA})_{44}$ (p-MBA: p-mercaptobenzoic acid, $SC_7O_2H_5$) (10), $Au_{25}(SCH_2CH_2Ph)_{18}^-$ (11–13), $Au_{38}(SCH_2CH_2Ph)_{24}$ (14), $Au_{36}(SPh\text{-}tBu)_{24}$ (15), $Au_{28}(SPh\text{-}tBu)_{20}$ (16), $Au_{20}(SPh\text{-}tBu)_{16}$ (17), $Au_{24\pm1}(SAdm)_{16}$ (18), and $Au_{18}(SC_6H_{11})_{14}$ (19). The lack of atomic structures of many RS-AuNPs has largely hindered a comprehensive understanding of the structure-property relationship of RS-AuNPs. Hence, a new experimental technique that can detect the atomic structures of AuNPs without the need for crystallization of RS-AuNPs is greatly desired.

Recently, Azubel et al. (20) have reported the atomic structure of an RS-AuNP containing 68 Au atoms determined by the powerful single-particle transmission electron microscopy (SP-TEM) combined with density-functional theory (DFT) computation and absorption spectroscopy. This SP-TEM–centered approach is transformative in the structure determination of AuNPs because it no longer requires producing a single crystal of RS-AuNPs. Nevertheless, thus far, SP-TEM can only yield the positions of heavy (that is, gold) atoms. Thus, structure determination of the protection ligands requires theoretical input from DFT computation and absorption spectroscopy measurement. According to the atomic positions of Au determined from SP-TEM,

the structure of $Au_{68}(SH)_{32}$ has been suggested (20) where some gold-thiolate motifs, such as bridging thiolates and ring-like structures, are predicted. In this communication, we present a series of new low-energy isomers in which the pattern of thiolate ligands on the gold core is determined according to the generic formulation (or rule) of the "divide and protect" (D&P) concept (7, 21). DFT optimization indicates that all the new isomers are uniformly lower in energy by 3 to 4 eV than the state-of-the-a.rt low-energy isomer reported in (20).

We note that the D&P approach combined with the DFT computation has been proven as a viable theoretical approach to predict low-energy or even global minimum structures of RS-AuNPs (22–29). The D&P approach elucidates that highly stable AuNPs tend to have a symmetric gold core covered by various levels of interfacial -RS-Au-RS-staple motifs (7). The lengths (or levels) of staples can vary, but overall they must obey two stoichiometry constraints for a given number of Au atoms in the inner core and in the ligand-core interface (7, 26). The validation of the D&P concept has been confirmed by the conceptual breakthrough (for example, the staple motifs for the ligand structures) being made in the total structure determination of the $Au_{102}(p\text{-MBA})_{44}$ by Kornberg and co-workers via x-ray crystallography (10), as well as the total structure determination of relatively small-sized clusters, such as $Au_{25}(SCH_2CH_2Ph)_{18}^-$ (11–13).

RESULTS AND DISCUSSION

First, on the basis of the precise positions of all Au atoms in the inner gold core and in the interface region of the Au_{68}NP determined from the SP-TEM experiment (20), we construct a number of different ligand structures with various levels of S-Au-S staple motifs, following the generic rule of the D&P approach (7). The generic rule states that an RS-AuNP can be divided into several groups as illustrated by $[Au]_{a\ +\ a'}[Au(SR)_2]_b\ [Au_2(SR)_3]_c$, where a, a', b, and c are integers. Here, $[Au]_{a\ +\ a'}$ represents the gold core, which satisfies the constraint condition that the number of "surface" Au atoms (a') in the gold core equals the sum of end points of the exterior motifs ($2b + 2c$); that is, each surface Au atom of the gold core is protected by one end point of the staple motif. Hence, the parameters a, a', b, and c for

[1]Division of Interfacial Water and Key Laboratory of Interfacial Physics and Technology, Shanghai Institute of Applied Physics, Chinese Academy of Sciences, Shanghai 201800, China. [2]Department of Chemistry and Nebraska Center for Materials and Nanoscience, University of Nebraska-Lincoln, Lincoln, NE 68588, USA.
*Corresponding author: E-mail: gaoyi@sinap.ac.cn (Y.G.); xzeng1@unl.edu (X.C.Z.)

$Au_{68}(SH)_{32}$ must satisfy $a + a' + b + 2c = 68$, $2b + 3c = 32$, and $a' = 2b + 2c$. Four initial core structures $[Au]_{a + a'}(a + a' = 48$ to $51)$ are examined, and each was covered by a certain number of -HS-Au-HS- and -HS-Au- HS-Au-HS- staple motifs: (i) $[Au]_{24+24}[Au(SR)_2]_4[Au_2(SR)_3]_8$, (ii) $[Au]_{23+26}[Au(SR)_2]_7[Au_2(SR)_3]_6$, (iii) $[Au]_{22+28}[Au(SR)_2]_{10}[Au_2(SR)_3]_4$, (iv) $[Au]_{21+30}[Au(SR)_2]_{13}[Au_2(SR)_3]_2$. The four newly constructed isomer structures together with the previously reported isomer based on the SP-TEM experiment (20) were optimized using the DFT method implemented in Materials Studio Dmol³ 7.0 (30, 31). The generalized gradient approximation with the Perdew-Burke-Ernzerhof (PBE) (32) functional and the double numeric polarized (DNP) basis set were adopted. Lastly, the linear and quadratic synchronous transit (LST/QST) method (33, 34) was used to locate the transition state of CO oxidation on $Au_{68}(SH)_{32}$. The theoretical powder x-ray diffraction (XRD) curve is calculated using the Debye formula:

$$I(s) = \sum_i \sum_{j\neq i} \frac{\cos\theta}{(1 + \alpha \cos(2\theta))} \exp\left(-\frac{Bs^2}{2}\right) f_i f_j \frac{\sin(2\pi d_{ij})}{2\pi d_{ij}}$$

where s is the diffraction vector length and θ is the scattering angle, satisfying $s = 2\sin\theta/\lambda$. λ and α are determined by the experimental setup and are set to be 0.1051967 nm and 1.01, respectively. B is the damping factor, which reflects thermal vibrations, and is set to be 0.03 nm². The corresponding atomic numbers are used for the scattering factor f_i. d_{ij} is the distance between atoms i and j. The atomic distance d_{ij} used in the calculation is taken from the optimized structure of clusters.

The optimized structures of the four isomers, **Iso1** to **Iso4**, classified by group divisions (i) to (iv), are shown in Fig. 1. The computed total energies of **Iso1** to **Iso4** are 3.95, 3.28, 3.31, and 3.06 eV, respectively, lower than the state-of-the-art low-energy isomer reported (20). The isomer **Iso1** appears to be the most stable isomer. The large energy difference between **Iso1** and the previously reported isomer indicates that the ligand patterns that can meet the generic formulation of the D&P approach are energetically much more favorable. In **Iso1** to **Iso4**, the 68 gold atoms can be grouped into an Au_{15} core with an Au atom in the center. Figure 2 displays two orthogonal views of the Au_{15} core in **Iso1** to **Iso4** and the Au_{15} core taken from the previously reported experimental isomer. In addition, the root mean square deviation (RMSD) values as a measure of deviation of the Au_{15} core in **Iso1** to **Iso4** from the experimental structure are presented in Table 1. The small RMSD values (about 0.3 Å) indicate that the overall structures of Au_{15} inner cores in **Iso1** to **Iso4** are consistent with the experimental one. Moreover, the structural distortion of the Au_{15} core in all five isomers can be recognized in Fig. 2. The slight distortion is probably induced by the different interfacial -RS-Au-RS- staple structures. As such, the core structure of Au_{68}NP is slightly distorted rather than being highly symmetric.

The fcc-like gold frameworks in **Iso1** to **Iso4** were singled out in Fig. 3. Here, to illustrate the fcc-like structure of gold frameworks more clearly, a common neighbor analysis (CNA) (35) was undertaken. Detailed information of CNA is given in table S1. The distinct CNA signatures

demonstrate that the inner gold core structures of **Iso1** to **Iso4** exhibit the fcc (100) and (111) surfaces, consistent with the SP-TEM experiment. The analysis of the Au_{15} core and the fcc-like framework suggests that the interior structures of **Iso1** to **Iso4** are consistent with the SP-TEM experiment. The RMSD values (about 0.7 Å) for the Au_{68} structures of **Iso1** to **Iso4**, however, become larger after including the surface Au atoms, as shown in Table 1, suggesting that the positions of the surface Au atoms that bind with the end point of the exterior motifs differ from those in the reported isomer. We note that in the SP-TEM experiment, a minimal electron dose was used (20). Could the
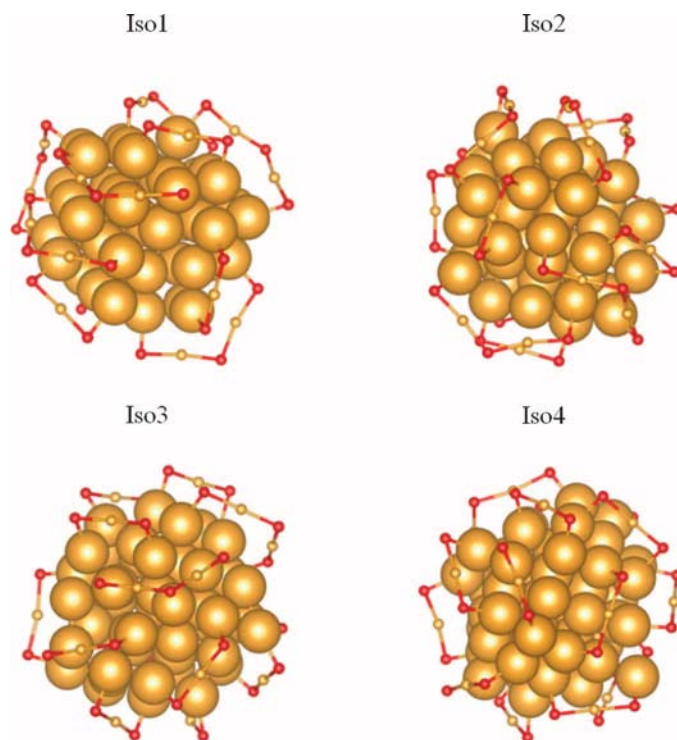

Fig. 1. Optimized structures of the four isomers Iso1 to Iso4 of Au₆₈(SH)₃₂. The Au and S atoms are in gold and red, respectively. The H atoms are not shown.
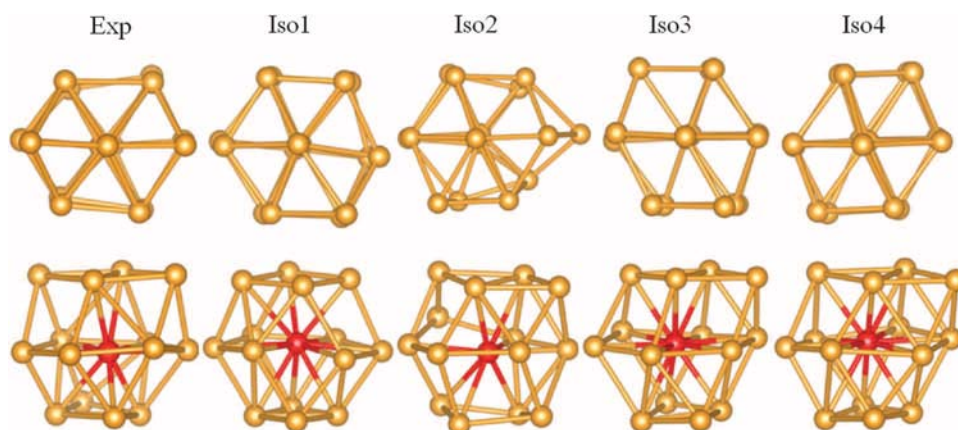
Fig. 2. Two orthogonal views of the 15 Au atoms in the core of the reported isomer from the SP-TEM experiment of Au₆₈ and in the cores of Iso1 to Iso4. The Au atom in the center is in red.

Table 1. RMSD values as a measure of the deviation of the Au$_{15}$ core and Au$_{68}$ in Iso1 to Iso4 from the experimental structure. The unit is in angstrom.
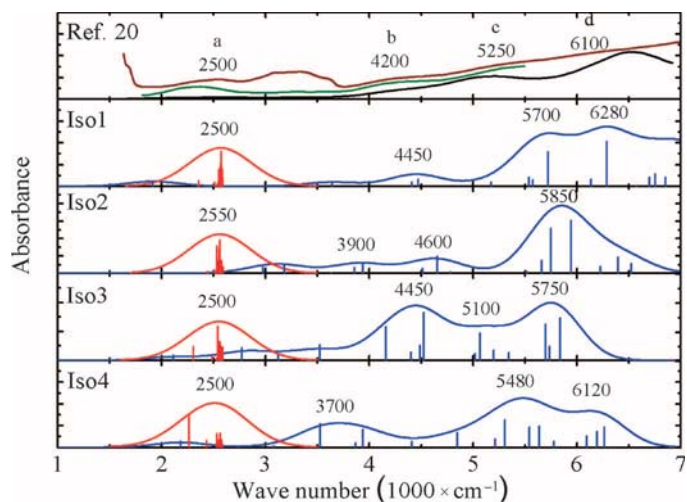
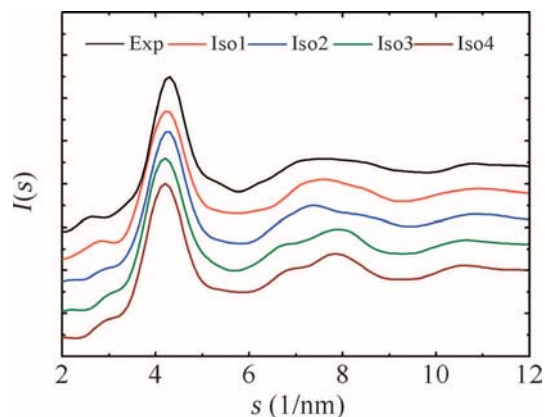|	Iso1	Iso2	Iso3	Iso4
Au$_{15}$	0.28	0.28	0.33	0.32
Au$_{68}$	0.70	0.71	0.69	0.69

Iso1 Iso2

Iso3 Iso4
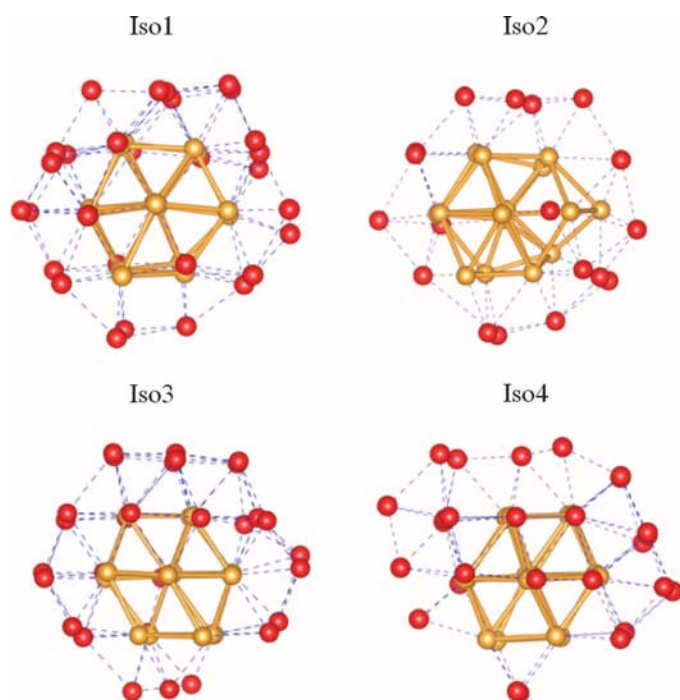
Fig. 3. The fcc-like frameworks of Au$_{68}$ in Iso1 to Iso4. The 15 Au atoms in the core are in gold, and the other Au atoms are in red.

Fig. 4. Optical absorption spectra of Au$_{68}$(SH)$_{32}$. Top row: The experimental (wine and olive) curves and the theoretical (black) curve plotted by taking the data from Ref. 20. **Rows 2** to **5:** Computed optical absorption spectra of **Iso1** to **Iso4**. The red curve denotes the vibrational frequency analysis based on the individual vibrational intensities (red vertical lines). The blue curve denotes spectra from TD-DFT computation of the individual optical transitions. In all five rows, the locations of four prominent absorption peaks (a, b, c, and d), from either experiment or theory, are displayed.

Fig. 5. Simulated XRD curves of Iso1 to Iso4 and the experimental Au$_{68}$(SH)$_{32}$ cluster.

TEM electron beam alter the positions of several surface Au atoms during the measurement? This question can be addressed through further experimental investigation using known RS-AuNP structures resolved from x-ray crystallography as a benchmark.

Computed optical absorption spectra of **Iso1** to **Iso4**, using the time-dependent DFT (TD-DFT) method, are shown in Fig. 4. As a comparison, both experimental and theoretical spectra of the previously reported isomer (20) are also included in Fig. 4. The locations of four prominent absorption peaks (a, b, c, and d) show that the computed optical absorption spectra of **Iso1** to **Iso4** are largely consistent with the experimental spectrum. Additionally, the simulated XRD curves of **Iso1** to **Iso4** and the experimental cluster (20) are shown in Fig. 5. Overall, **Iso1** results in the best agreement with the experimental curve. For **Iso2** to **Iso4**, their first, second, and third peaks are slightly shifted compared to the corresponding experimental peaks. Further analysis of the molecular orbital (MO) levels and the corresponding atomic orbital components in each MO of **Iso1** to **Iso4** are presented in figs. S1 to S4. We find that the strong absorption peaks b to d are mainly contributed by the core [Au]$_{a + a'}$ ($a + a'$ = 48 to 51). Overall, the positions of the major absorption peaks of these five isomers are more or less similar to one another because they have similar core structures. However, as shown in Fig. 4, the shape of the computed absorption curves of **Iso1** to **Iso4** are different, suggesting that the overall shape of the optical absorption spectrum of Au$_{68}$(SH)$_{32}$ is sensitive to the isomer structure.

Finally, we examine catalytic properties of Au$_{68}$(SH)$_{32}$ by using the CO oxidation as a probe. The computed catalytic reaction pathway for the CO oxidation on the **Iso1** cluster is shown in Fig. 6. Because all gold atoms in the clusters are protected by the thiolate groups, several surface staple motifs of **Iso1** are removed to make the catalytic reaction, as indicated in previous studies (36, 37). As shown in Fig. 6, the CO and O$_2$ molecules can be favorably coadsorbed on two neighboring low-coordinated Au atoms, with the coadsorption energy of CO$_2$ and O$_2$ being about −1.24 eV. Upon the coadsorption of CO and O$_2$, the two molecules can move closer while the O-O bond length is elongated.
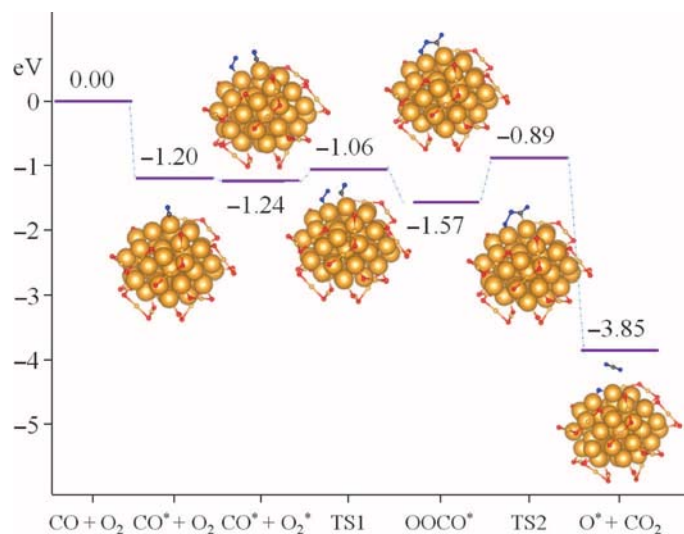
Fig. 6. Computed reaction pathway for the CO oxidation on Iso1 cluster. Here, the symbol * denotes adsorption of the corresponding molecules on Au atoms. Au, S, C, and O atoms are in gold, red, gray, and blue, respectively. H atoms are not shown.

In the first step, a relatively low-energy barrier of 0.18 eV (TS1 in Fig. 6) can be overcome while the two molecular species arrive at a bridge-like metastable intermediate state characterized by the O-C-O-O species, with the O–O bond length being 1.43 Å. In the second step, the O–O bond length is further elongated to 1.85 Å while CO fully grasps an O atom of O_2 to form a CO_2 molecule. Lastly, CO_2 desorbs with cleaving the O–O bond, leaving the other O atom adsorbed on the gold cluster. The second step (TS2 in Fig. 6) is the rate-determining step that requires overcoming a reaction barrier of 0.68 eV. These reaction barriers are comparable to those of typical nanogold catalysts (38–40), indicating that the Au_{68} cluster can be a stand-alone nanoscale catalyst for future applications.

CONCLUSION

We have presented a series of new low-energy isomer structures of $Au_{68}(SH)_{32}$ determined from the generic formulation of the D&P approach. The consistency in the interior structure of Au_{68} and the peak locations of the optical absorption spectra between the new isomers and the isomer reported from the SP-TEM experiment suggests that these isomers, **Iso1** in particular, are promising candidates for the most stable atomic structure of $Au_{68}(SH)_{32}$. Further computation of catalytic properties of $Au_{68}(SH)_{32}$ toward CO oxidation suggests that this magic number cluster can be a stand-alone nanoscale catalyst for future applications. Confirmation of the predicted staple motif–based atomic structure of $Au_{68}(SH)_{32}$ must await future benchmark experiments, for example, using known staple motif–based RS-AuNPs, such as $Au_{102}(p\text{-MBA})_{44}$, as a benchmark in future SP-TEM experiment.

SUPPLEMENTARY MATERIALS

Supplementary material for this article is available at http://advances.sciencemag.org/cgi/content/full/1/3/e1400211/DC1

Fig. S1. MO energy level diagram for **Iso1**, with the three peaks b, c, and d in Fig. 4 being assigned to various excitation modes.

Fig. S2. MO energy level diagram for **Iso2**, with the three peaks b, c, and d in Fig. 4 being assigned to various excitation modes.
Fig. S3. MO energy level diagram for **Iso3**, with the three peaks b, c, and d in Fig. 4 being assigned to various excitation modes.
Fig. S4. MO energy level diagram for **Iso4**, with the three peaks b, c, and d in Fig. 4 being assigned to various excitation modes.
Table S1. Bond CNA signatures for **Iso1** to **Iso4**.
Coordinate files

REFERENCES AND NOTES

1. R. Jin, Quantum sized, thiolate-protected gold nanoclusters. *Nanoscale* **2**, 343–362 (2010).
2. M. M. Alvarez, J. T. Khoury, T. G. Schaaff, M. N. Shafigullin, I. Vezmar, R. L. Whetten, Optical absorption spectra of nanocrystal gold molecules. *J. Phys. Chem. B* **101**, 3706–3712 (1997).
3. Y. Negishi, K. Nobusada, T. Tsukuda, Glutathione-protected gold clusters revisited:Bridging the gap between gold(i)–thiolate complexes and thiolate-protected gold nanocrystals. *J. Am. Chem. Soc.* **127**, 5261–5270 (2005).
4. S. Chen, R. S. Ingram, M. J. Hostetler, J. J. Pietron, R. W. Murray, T. G. Schaaff, J. T. Khoury, M. M. Alvarez, R. L. Whetten, Gold nanoelectrodes of varied size: Transition to molecule-like charging. *Science* **280**, 2098–2101 (1998).
5. A. S. K. Hashmi, G. J. Hutchings, Gold catalysis. *Angew. Chem. Int. Ed. Engl.* **45**, 7896–7936 (2006).
6. H. Häkkinen, The gold–sulfur interface at the nanoscale. *Nat. Chem.* **4**, 443–455 (2012).
7. Y. Pei, X. C. Zeng, Investigating the structural evolution of thiolate protected gold clusters from first-principles. *Nanoscale* **4**, 4054–4072 (2012).
8. H. Qian, M. Zhu, Z. Wu, R. Jin, Quantum sized gold nanoclusters with atomic precision. *Acc. Chem. Res.* **45**, 1470–1479 (2012).
9. S. Knoppe, I. Dolamic, A. Dass, T. Burgi, Separation of enantiomers and CD spectra of $Au_{40}(SCH_2CH_2Ph)_{24}$: Spectroscopic evidence for intrinsic chirality. *Angew. Chem. Int. Ed. Engl.* **51**, 7589–7591 (2012).
10. P. D. Jadzinsky, G. Calero, C. J. Ackerson, D. A. Bushnell, R. D. Kornberg, Structure of a thiol monolayer-protected gold nanoparticle at 1.1 Å resolution. *Science* **318**, 430–433 (2007).
11. M. W. Heaven, A. Dass, P. S. White, K. M. Holt, R. W. Murray, Crystal structure of the gold nanoparticle $[N(C_8H_{17})_4][Au_{25}(SCH_2CH_2Ph)_{18}]$. *J. Am. Chem. Soc.* **130**, 3754–3755 (2008).
12. J. Akola, M. Walter, R. L. Whetten, H. Häkkinen, H. Grönbeck, On the structure of thiolate-protected Au25. *J. Am. Chem. Soc.* **130**, 3756–3757 (2008).
13. M. Zhu, C. M. Aikens, F. J. Hollander, G. C. Schatz, R. Jin, Correlating the crystal structure of a thiol-protected Au25 cluster and optical properties. *J. Am. Chem. Soc.* **130**, 5883–5885 (2008).
14. H. Qian, W. T. Eckenhoff, Y. Zhu, T. Pintauer, R. Jin, Total structure determination of thiolate-protected Au38 nanoparticles. *J. Am. Chem. Soc.* **132**, 8280–8281 (2010).
15. C. Zeng, H. Qian, T. Li, G. Li, N. L. Rosi, B. Yoon, R. N. Barnett, R. L. Whetten, U. Landman, R. Jin, Total structure and electronic properties of the gold nanocrystal $Au_{36}(SR)_{24}$. *Angew. Chem. Int. Ed. Engl.* **51**, 13114–13118 (2012).
16. C. Zeng, T. Li, A. Das, N. L. Rosi, R. Jin, Chiral structure of thiolate-protected 28-gold-atom nanocluster determined by x-ray crystallography. *J. Am. Chem. Soc.* **135**, 10011–10013 (2013).
17. C. Zeng, C. Liu, Y. Chen, N. L. Rosi, R. Jin, Gold-thiolate ring as a protecting motif in the $Au_{20}(SR)_{16}$ nanocluster and implications. *J. Am. Chem. Soc.* **136**, 11922–11925 (2014).
18. D. Crasto, G. Barcaro, M. Stener, L. Sementa, A. Fortunelli, A. Dass, $Au_{24}(SAdm)_{16}$ nanomolecules: X-ray crystal structure, theoretical analysis, adaptability of adamantane ligands to form $Au_{23}(SAdm)_{16}$ and $Au_{25}(SAdm)_{16}$, and its relation to $Au_{25}(SR)_{18}$. *J. Am. Chem. Soc.* **136**, 14933–14940 (2014).
19. A. Das, C. Liu, H. Y. Byun, K. Nobusada, S. Zhao, N. Rosi, R. Jin, Structure determination of $[Au_{18}(SR)_{14}]$. *Angew. Chem. Int. Ed. Engl.* **54**, 3140–3144 (2015).
20. M. Azubel, J. Koivisto, S. Malola, D. Bushnell, G. L. Hura, A. L. Koh, H. Tsunoyama, T. Tsukuda, M. Pettersson, H. Häkkinen, R. D. Kornberg, Electron microscopy of gold nanoparticles at atomic resolution. *Science* **345**, 909–912 (2014).
21. H. Häkkinen, M. Walter, H. Gronbeck, Divide and protect: Capping gold nanoclusters with molecular gold–thiolate rings. *J. Phys. Chem. B* **110**, 9927–9931 (2006).
22. D. E. Jiang, M. Walter, J. Akola, On the structure of a thiolated gold cluster: $Au_{44}(SR)_{28}^{2-}$. *J. Phys. Chem. C* **114**, 15883–15889 (2010).
23. O. Lopez-Acevedo, J. Akola, R. L. Whetten, H. Gronbeck, H. Häkkinen, Structure and bonding in the ubiquitous icosahedral metallic gold cluster $Au_{144}(SR)_{60}$. *J. Phys. Chem. C* **113**, 5035–5038 (2009).
24. D. E. Jiang, R. L. Whetten, W. D. Luo, S. Dai, The smallest thiolated gold superatom complexes. *J. Phys. Chem. C* **113**, 17291–17295 (2009).
25. A. Tlahuice, I. L. Garzon, On the structure of the $Au_{18}(SR)_{14}$ cluster. *Phys. Chem. Chem. Phys.* **14**, 3737–3740 (2012).
26. Y. Pei, Y. Gao, X. C. Zeng, Structural prediction of thiolate-protected Au38: A face-fused bi-icosahedral Au core. *J. Am. Chem. Soc.* **130**, 7830–7832 (2008).

27. Y. Pei, Y. Gao, N. Shao, X. C. Zeng, Thiolate-protected $Au_{20}(SR)_{16}$ cluster: Prolate Au_8 core with new $[Au_3(SR)_4]$ staple motif. *J. Am. Chem. Soc.* **131**, 13619–13621 (2009).

28. Y. Pei, R. Pal, C. Liu, Y. Gao, Z. Zhang, X. C. Zeng, Interlocked catenane-like structure predicted in $Au_{24}(SR)_{20}$: Implication to structural evolution of thiolated gold clusters from homoleptic gold(I) thiolates to core-stacked nanoparticles. *J. Am. Chem. Soc.* **134**, 3015–3024 (2012).

29. D. E. Jiang, Staple Fitness: A concept to understand and predict the structures of thiolated gold nanoclusters. *Chemistry* **17**, 12289–12293 (2011).

30. B. Delley, An all-electron numerical method for solving the local density functional for polyatomic molecules. *J. Chem. Phys.* **92**, 508–517 (1990).

31. B. Delley, From molecules to solids with the $DMol^3$ approach. *J. Chem. Phys.* **113**, 7756–7764 (2000). $Dmol^3$ is available from Biovia.

32. J. P. Perdew, K. Burke, M. Ernzerhof, Generalized gradient approximation made simple. *Phys. Rev. Lett.* **77**, 3865–3868 (1996).

33. T. A. Halgren, W. N. Lipscomb, The synchronous-transit method for determining reaction pathways and locating molecular transition states. *Chem. Phys. Lett.* **49**, 225–232 (1977).

34. C. Y. Peng, H. B. Schlegel, Combining synchronous transit and quasi-Newton methods for finding transition states. *Isr. J. Chem.* **33**, 449–454 (1993).

35. C. L. Cleveland, W. D. Luedtke, U. Landman, Melting of gold clusters. *Phys. Rev. B* **60**, 5065–5077 (1999).

36. O. Lopez-Acevedo, K. A. Kacprzak, J. Akola, H. Häkkinen, Quantum size effects in ambient CO oxidation catalysed by ligand-protected gold clusters. *Nat. Chem.* **2**, 329–334 (2010).

37. Z. Wu, D. Jiang, A. K. P. Mann, D. R. Mullins, Z. Qiao, L. F. Allard, C. Zeng, R. Jin, S. H. Overbury, Thiolate ligands as a double-edged sword for CO oxidation on CeO_2 supported $Au_{25}(SCH_2CH_2Ph)_{18}$ nanoclusters. *J. Am. Chem. Soc.* **136**, 6111–6122 (2014).

38. H. Li, L. Li, A. Pedersen, Y. Gao, N. Khetrapal, H. Jónsson, X. C. Zeng, Magic-number gold nanoclusters with diameters from 1 to 3.5 nm: Relative stability and catalytic activity for CO oxidation. *Nano Lett.* **15**, 682–688(2015).

39. Y. Gao, N. Shao, Y. Pei, Z. Chen, X. C. Zeng, Catalytic activities of subnanometer gold clusters (Au16-Au18, Au20, and Au27-Au35) for CO oxidation. *ACS Nano* **5**, 7818–7829 (2011).

40. C. Liu, Y. Tan, S. Lin, H. Li, X. Wu, L. Li, Y. Pei, X. C. Zeng, CO self-promoting oxidation on nanosized gold clusters: Triangular Au3 active site and CO induced O-O scission. *J. Am. Chem. Soc.* **135**, 2583–2595 (2013).

Citation: W. W. Xu, Y. Gao, X. C. Zeng, Unraveling structures of protection ligands on gold nanoparticle $Au_{68}(SH)_{32}$. *Sci. Adv.* **1**, e1400211 (2015).